arXiv:1704.08477v1 [cond-mat.mes-hall] 27 Apr 2017

Revealing large-scale homogeneity and trace impurity sensitivity of GaAs nanoscale membranes

Z. Yang,[†] A. Surrente,[†] G. Tutuncuoglu,[‡] K. Galkowski,[†,§] M. Cazaban-Carrazé ,[†] F. Amaduzzi,[‡] P. Leroux,[¶] D. K. Maude,[†] A. Fontcuberta i Morral,[*,‡] and P. Plochocka[*,†]

†*Laboratoire National des Champs Magnétiques Intenses, CNRS-UGA-UPS-INSA, 143, avenue de Rangueil, 31400 Toulouse*

‡*Laboratory of Semiconductor Material, Ecole Polytechnique Fédérale de Lausanne, Lausanne, Switzerland*

¶*Laboratory of Semiconductor Material, École Polytechnique Fédérale de Lausanne, Lausanne, Switzerland*

§*Institute of Experimental Physics, Faculty of Physics, University of Warsaw - Pasteura 5, 02-093 Warsaw, Poland*

E-mail: anna.fontcuberta-morral@epfl.ch; paulina.plochocka@lncmi.cnrs.fr

Abstract

III-V nanostructures have the potential to revolutionize optoelectronics and energy harvesting. For this to become a reality, critical issues such as reproducibility and sensitivity to defects should be resolved. By discussing the optical properties of MBE grown GaAs nanomembranes we highlight several features that bring them closer to large scale applications. Uncapped membranes exhibit a very high optical quality,

expressed by extremely narrow neutral exciton emission, allowing the resolution of the more complex excitonic structure for the first time. Capping of the membranes with an AlGaAs shell results in a strong increase of emission intensity but also to a shift and broadening of the exciton peak. This is attributed to the existence of impurities in the shell, beyond MBE-grade quality, showing the high sensitivity of these structures to the presence of impurities. Finally, emission properties are identical at the sub-micron and sub-millimeter scale, demonstrating the potential of these structures for large scale applications.

Keywords: GaAs/AlGaAs nano mebranes, photoluminescence, electronic and optical properties of ensemble vs single nano membrane

Nanowires (NWs) are filamentary crystals with a diameter in the sub-micrometer down to nanometer range. Their special morphology, dimensions and high surface-to-volume ratio are often translated into advantageous optical and electrical properties. As a consequence, they have been widely used in electronics,[1–5] optoelectronics,[6,7] solar cells[8–11] and sensors.[12,13] If not adequately passivated, the surface recombination can limit the optical performance of the NWs.[14] In addition, surface depletion can also affect the volume distribution and separation of the carriers in the NW.[15–19] Different passivation methods have been employed in the past, notably capping of the free surfaces with a higher bandgap shell around the nanowire.[20–22] Nevertheless, capping also modifies the nature of the surface. Several effects have been reported, such as band bending at the interface leading to the accumulation of the charge at the interface or piezo electric strain.[23–27] In addition, the AlGaAs alloy typically used for capping GaAs nanowires is generally inhomogeneous, with directed and random segregation of Ga and Al forming respectively Al-rich ridges and Ga-rich nanoscale islands .[28,29] Simultaneously, III-V NWs can suffer from twin defects and polytypism,[30,31] which adversely affect their electronic and optical properties.[32–34] With a judicious optimization of growth conditions, single NWs with a pure zinc-blende or wurzite structure can be obtained.[35–37] Still, the optical and electronic properties tend to fluctuate considerably from NW to NW,

which precludes the proper control of the response of an ensemble of nanowires.

Recently, alternative approaches to obtain defect-free nano structures have been proposed. Particularly promising is the inversion of polarity from B to A as well as template assisted and nano-membrane assisted selective epitaxy (TASE and MASE, respectively). All these techniques provide defect free III-V nano structures by blocking the formation of twinning defects.[38–43] An additional advantage of these approaches is the possibility to engineer the shape, so that membranes,[43] sails[42] or sheets[39,41] can be grown. Nanoscale membranes show relatively long minority carrier diffusion length of 180 nm at 4.2 K, which is significantly larger than the diffusion lengths found in nanowires.[40,41] Moreover, by introducing passivation and/or doped structures, the design can be further sophisticated.[40,41] The transfer of NW optoelectronic devices to industry requires achieving highly reproducible and uniform structures through a large surface area, so that the properties of ensemble and single object are indistinguishable. For instance, in photoluminescence this implies indistinguishability in terms of line width and emission energy and spectral shape. Growing the nano structures using TASE and MASE turned out to be the most promising direction to achieve large area highly uniform systems.

In this work we demonstrate, by using optical techniques, that GaAs nanoscale membranes provide the settings for extremely high quality nanostructures, both from the structural and functional point of view. We elucidate how the improvement in functional properties is homogeneous across the whole wafer. This shows the potential of these nanostructures for nanotechnology and opens the path towards large scale nano-manufacturing. Furthermore, we provide very strong evidence that capping of the membranes, despite increasing the emission efficiency, unexpectedly leads to the degradation of their optical properties.

Nanomembranes have been grown using selective area epitaxy (for growth details see methods and reference[43]). In Fig. 1(a) a tilted SEM image of a GaAs nanomembrane array consisting of 10μm long and 100 nm wide nanomembranes with 500 nm pitch, used in the further optical experiments, are shown. Pitch is defined as the distance between the mem-

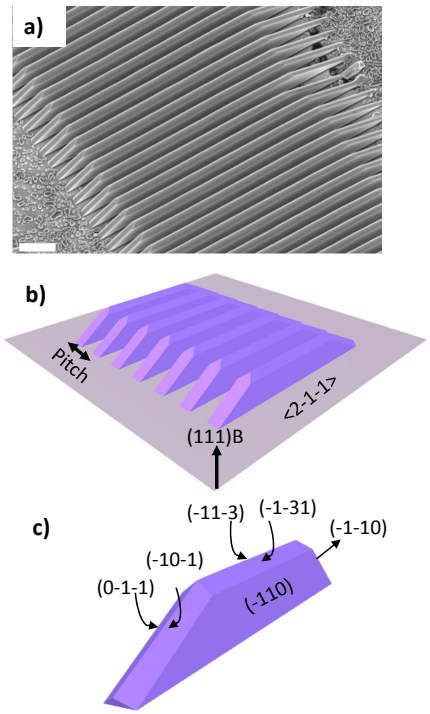

Figure 1: (a) 20° tilted SEM image of a GaAs nano membrane array (b) 3D model of the membrane array signifying the orientation of the structures (c) Faceting of a GaAs membrane.

branes, as depicted in Fig. 1(b). Nanomembranes are oriented in $\langle 2\bar{1}\bar{1}\rangle$ direction which is perpendicular to (111)B and $(\bar{1}\bar{1}0)$ directions and expose the facets shown in Figure 1(c). Most of the facets belong to {110} family except high index top facets of $(\bar{1}1\bar{3})$ and $(\bar{1}\bar{3}1)$. Adjusting the membrane orientation to $\langle 2\bar{1}\bar{1}\rangle$ and growth conditions, it is possible to obtain pure zinc-blende structures with high-aspect ratio with Molecular Beam Epitaxy (MBE).[43] Detailed growth conditions are given in the Method section. The reported shape is the result of an hour growth with 1 Å/s growth rate. If growth is continued long enough, the morphology of the membrane evolves into a triangular shape. During the growth of AlGaAs shell the $(\bar{1}\bar{1}0)$ facet transforms to $(\bar{2}\bar{2}1)$.

Typical normalized μPL spectra of a single uncapped GaAs and capped GaAs/$Al_xGa_{1-x}As$ nano membranes are presented in Fig. 2(a). For the capped membranes the data have been taken for three different compositions of the shell ($x = 15, 33, 50\%$). Overall, the emission spectra are composed of two bands, around 1515 and 1490 meV. The higher energy band

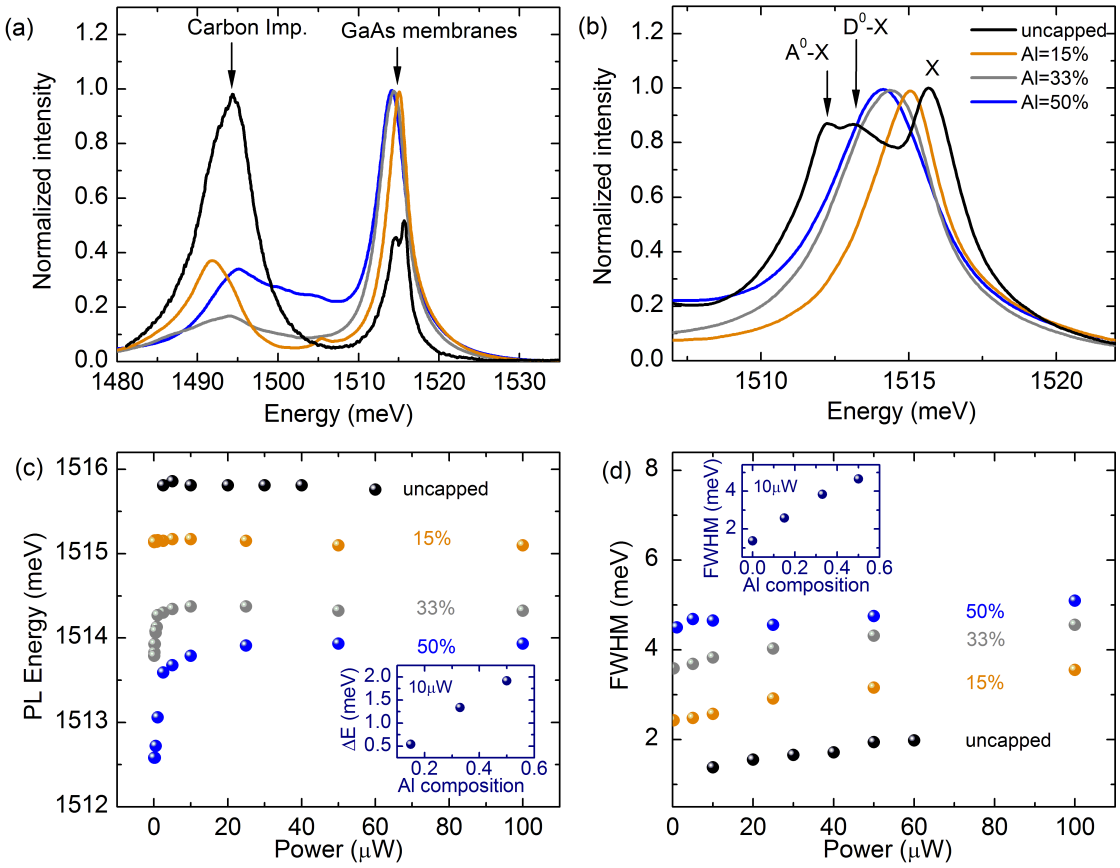

Figure 2: Normalized photoluminescence spectra of the uncapped GaAs and capped GaAs/AlGaAs nano membranes in a (a) wide (full) and (b) narrower (emission from the core) energy range. (c) Emission energy and (d) FWHM of the free exciton emission as a function of the excitation power. Red-shift of the PL for different Al composition is plotted as symbols in the inset in panel (c). The inset in panel (d) shows the evolution of the FWHM of the PL line for different Al composition in the shell.

corresponds to the band-edge luminescence of the GaAs membranes, while the lower energy emission can be attributed to the donor acceptor transitions due to carbon impurities normally present in commercial GaAs substrates,[44,45] which was further observed in detailed cathodoluminescence studies. Our spectra are comparable to previously reported optical emission in nano membranes with 33% Al composition in the shell.[43] The peak related to the carbon impurities can be used as a reference for the luminescence intensity. After capping, the emission from the GaAs membrane increases dominating the carbon related PL. The dramatic increase of the emission from the membrane is a direct consequence of the

surface passivation that reduces the non radiative surface recombination.

The detailed nature of the emission is very different for capped and uncapped samples. For uncapped membranes the spectrum is composed of three lines (see Fig2(b)). The peak at the highest energy of ~ 1515.5 meV corresponds to the free exciton emission, while the two peaks at lower energies are related to neutral donor bound exciton emission ($D^0 - X$) and acceptor bound exciton emission ($A^0 - X$) with emission energies which are typical for bulk GaAs .[46,47] This result rules out any possible quantum confinement in the nano membranes. This is not unexpected since the exciton Bohr radius of $\simeq 14\,\mathrm{nm}$ in GaAs is much smaller than the size of the membrane.[48] In contrast, the typical emission spectra for the GaAs nano membranes capped with $Al_xGa_{1-x}As$ layer (Fig. 2(b)) are composed of a single line, which we attribute to the neutral exciton recombination. Emission lines from $D^0 - X$ and $A^0 - X$ are completely absent. The neutral exciton emission energy red shifts and broadens with increasing Al shell content. To quantify this effect we have measured the power dependence of the energy and full width at the half maximum (FWHM) of the neutral exciton emission. In Fig 2(c) the emission energy is plotted as a function of excitation power. For membranes with high aluminium shell content ($x \geq 0.3$) a blue shift is observed with increasing excitation power which quickly saturates for powers above a few μW. For powers of 10μW and above the emission energy is independent of the excitation power. There is a clear and systematic decrease in the emission energy (red-shift) with increasing Al content. This is illustrated in the inset in the Fig. 2(c), where the energy difference between uncapped and capped emission ΔE is plotted as a function of the shell aluminium composition x for the same excitation power. In Fig. 2(d) the FWHM of the emission is plotted as a function of the excitation power. The line widths increase slightly with increasing power, but this is negligible compared to the increase in the FWHM with increasing Al content of the shell. In the inset of Fig. 2(d) we plot the FWHM versus the shell Al content for an excitation power of 10μW. The linewidth is multiplied by roughly a factor of 5 between the uncapped membrane and the membrane with a 50% Al content cap layer. Thus, while capping the

membranes reduces non-radiative surface recombination, leading to enhanced neutral exciton emission, it also detrimentally affects the optical properties of the GaAs core, leading to a significantly broadened emission.

We turn now to the effect of the red-shift of the excitonic emission upon capping the membranes with AlGaAs. In fact, a similar effect has been observed previously for a simple AlGaAs/GaAs interface,[23,49] InP nanowires,[50] and for GaAs nanowires capped with AlGaAs shell .[24,26,27] For simple AlGaAs/GaAs the band bending at the interface forms a pocket for the electrons or holes .[23,49] Such confined carriers at the interface will recombine with the free carriers (of the opposite species) in the valence or conduction band at a sufficient distance from the interface that flat-band conditions have been re-established. As the charges are spatially separated, emission has a spatially indirect character and is red shifted in comparison to the simple excitonic emission observed in uncapped GaAs. Moreover, the band bending can be screened by photo created carriers decreasing the overall effect with the increase of the excitation power. For InP nanowires a similar picture has been proposed, where the band bending was induced by a pinning of the Fermi level.[50] Finally, for GaAs nanowires capped with AlGaAs shell, the mechanism of the band bending can be enriched by strain, related to the shell thickness.[26,27] However, the strain plays a significant role only for rather thick shells. In the case of the nano membranes the core is much thicker than the shell. Additional confirmation of the negligible role of the strain in our structures is given by the Raman spectroscopy. If the shift we observe originated from strain, it would imply a significantly lower Al composition than the nominal composition.[51] Our Raman measurements, (see SI), confirm that the Al composition corresponds very well to the nominal composition in the nano membranes and the lack of strain in the membrane core.

We attribute the observed red shift of the emission to the indirect nature of the exciton recombination at the capping interface. Due to residual doping in the AlGaAs shell, band bending occurs at the AlGaAs/GaAs interface. To this end, we illustrate in Fig 3(a) the position of the valence and conduction band edges as a function of the distance from the

membrane surface. Our hypothesis is that the AlGaAs shell contains some oxygen impurities, associated with the addition of aluminum. Secondary ion mass spectroscopy measurements on AlGaAs layers indeed indicate a slight O-contamination associated with Aluminum (see SI). This contamination is still better than the purity specifications of MBE-grade Aluminum, 6N5, which implies that nanostructures are much more sensitive than bulk structures to impurities. Thus, the optical response of high quality nano structures provides a sensitive means to detects extremely low levels of impurities. The red-shift of the luminescence at high excitation powers is larger for higher Al content (see Figure 3(a)). This shows, that the band bending increases with the Al content in the shell as the exciton recombination becomes more indirect.

Our observations are further supported by the simulation of the band bending at the AlGaAs/GaAs interface by solving Poisson and Schrödinger equations self-consistently with the software nextnano3. In the model we have included the presence of p-type interface states between GaAs and AlGaAs shell, which increases with increasing Al content. Our experimental data fits well with 2×10^9, 6×10^9 and $8 \times 10^9\,\mathrm{cm}^{-2}$ interface dopants for an Al concentration of 15%, 30% and 50% respectively. Fig. 3(b) shows the resulting band bending at the tip of the membrane as a function of the distance to the surface and for the three Al contents. Here is evident the presence of a triangular potential in the valence band at the interface GaAs/AlGaAs where holes can be trapped. We can also observe an increase of the height of the potential with Al content, which results in a red-shift of the indirect transition.

It is worth noting, that the red shift observed in our samples is of comparable magnitude with that observed by Songmuang at al[26] but much smaller than that reported by Dhaka et al .[24] This discrepancy can be partly ascribed to the MetalOrganic Vapor Phase Epitaxy (MOVPE) employed by Dhaka et al [24] to grow their nanowires. MOVPE involves the use of metalorganic species as group III precursors, which might introduce an unintentionally high concentration of impurities.

The small blue shift observed at low powers, which saturates around 10μW has been

also observed for GaAs nanowires capped with AlGaAs shell[26,27] and it was associated with the presence of some negatively charged traps at the interface, which are filled by photo created carriers in the AlGaAs shell, which migrates towards interface. Once filled, they can no longer modify the band bending at the interface, which explains the saturation of the blue-shift of the emission energy above 10μW, indicating that the band bending is the dominant effect in our nanomembranes.

The special geometry of the nanoscale membranes requires some further modeling. First, the non-flat geometry of the interface should result into a spatially dependent band bending. In addition, the vertical nature of the membranes can additionally lead to non-homogeneous light absorption.[28] Fig. 3(c) shows the 2D valence and the conduction band maps for an Al concentration of 50%. We can observe a band-bending at the interface which is significantly larger at the top corner of the nanomembrane. We have simulated the electromagnetic field distribution using the package Meep, a freely available software implementing the Finite Difference in Time Domain Method [52] taking into consideration the exact geometry of the core/shell nanomembrane with a shell of 30% of Al. The dielectric constant is taken from Ref. [53]. Fig. 3(d) shows the cross-sectional map of the computed electric field energy density for a nanomembrane under the presence of a monochromatic wave coming from the top and with parallel polarization. It is clearly seen that the field energy is not distributed evenly across the cross-section but is rather confined at the top edge of the nanomembrane. This means that our μ photoluminescence experiments mainly probe the exciton properties at the tip, where the band bending is more pronounced. The results of this simulation explains also the broadening of the emission with the increasing Al content. Although emission is probed locally, the probed region can contain non homogenies band bending leading to the broadening of the emission peak. This is in perfect agreement with the observation that the effect is the strongest for the highest Al composition.

Finally, we come to perhaps the most striking and novel property of these nano membranes, namely their reproducibility and large scale uniformity. While epitaxial MBE pro-

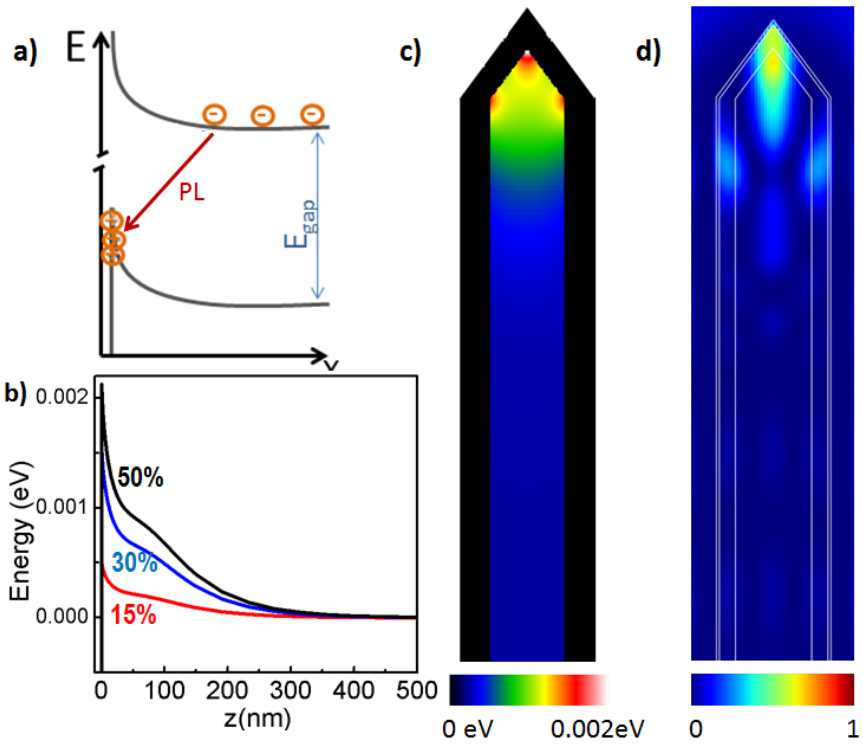

Figure 3: (a) The position of the valence and conduction band edges as a function of the distance from the membrane surface. b) Band bending at the tip of the membrane as a function of the distance to the surface and for the three Al contents. (c) 2D valence and the conduction band maps for an Al concentration of 50% (d) Cross-sectional map of the electric field energy density for a nanomembrane under the presence of a monochromatic wave coming from the top and with parallel polarization

vides highly uniform growth, this is not the case for the self organized growth of quantum dots or NWs, where nucleation events in growth follow poissonian statistics that lead to a distribution in the properties. As an example, in NWs this leads to a twinning or stacking fault density that varies from NW to NW (complete defect-free structures are rare). As a result, the optical properties vary from NW to NW and macro-photoluminescence measurements of the ensemble normally do not match micro photoluminescence of a single NW. We have recently shown that MBE growth using selective area epitaxy can produce arrays of defect free nano membranes.[43] However, optical investigations were limited to PL of a single nano membrane so that the uniform optical properties of an ensemble has never been

demonstrated.

To demonstrate large scale uniformity, we compare the emission spectra of a single membrane with the ensemble emission of around 250 membranes measured using macro PL, achieved here by defocussing the laser spot. Representative PL spectra are shown in Fig. 4 for the capped and uncapped membranes. Defocussing increases the contribution of the substrate which is reflected in the slightly increased amplitude of the carbon related emission which can be seen in Figure 4. The substrate PL is dominated by the carbon related emission and free exciton emission is not observed from the substrate. We have mapped the luminescence properties of the membranes by cathodoluminescence in a previous work.[43] These measurements confirm that the carbon-related peak originates solely from the substrate.

Surprisingly, the PL originating from single membrane is almost identical to the ensemble emission. The carbon impurity emission is slightly enhanced in the ensemble emission of the capped samples ($\simeq$ 20% for the 50% Al membrane). This is probably due to the inhomogeneous distribution of the carbon impurities across the substrate. In contrast, the neutral exciton emission is strictly identical in both the energy of the emission and the line width for all samples. In the uncapped sample, the neutral and bound exciton emission is also almost indistinguishable (see inset Figure 4(a)). The identical emission from a single and an ensemble of membranes unequivocally demonstrates the very high quality of the crystal structure and extremely high reproducibility of the nano membranes, which has never been observed for the classical radial nanowires. Moreover, data measured at different places on the same membrane, and on different membranes, vary very little in intensity, energy position or line width, suggesting an excellent crystal quality of the uncapped membranes.

In conclusion, we have demonstrated luminescence properties of GaAs membranes which are on a par with the best two-dimensional layers obtained with MBE. Upon capping of the membranes with an AlGaAs layer the PL emission is strongly enhanced, but also unexpectedly accompanied by a degradation of the optical properties with a significant broadening of the exciton emission. Capping also leads to a red shift of the emission which has been

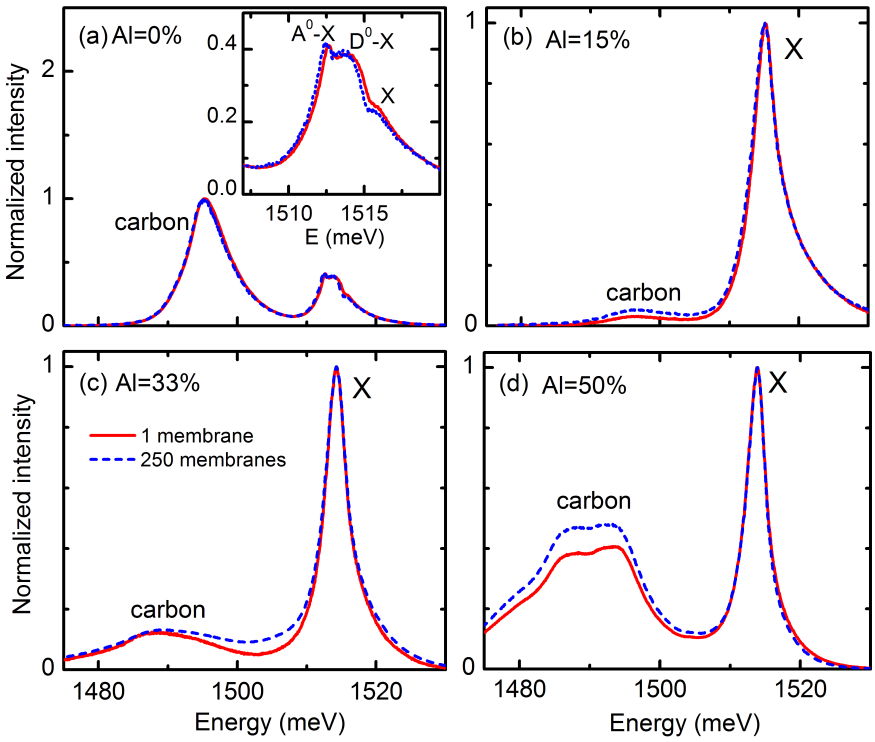

Figure 4: (a)-(d) Normalized photoluminescence spectra of the uncapped GaAs and capped GaAs/AlGaAs nano membranes measured at low temperature. The solid red and dashed blue line correspond to the excitation/emission from 1 and 250 membranes respectively. The inset shows the zoom of the GaAs core emission of the uncapped membranes.

attributed to the residual carbon doping of Al-containing layers which leads to band bending at the AlGaAs/GaAs interface. The quality of the membrane growth process is further supported by ensemble measurements, which are almost indistinguishable from the single membrane results. Additionally, our results show an extreme high sensitivity of the optical response of the nano membranes on impurities concentration that goes beyond what is possible in terms of state of the art high purity MBE.

ASSOCIATED CONTENT

Additional characterization of membranes, inelastic light scattering (Raman), secondary ion mass spectroscopy (SIMS) profile (PDF).

ACKNOWLEDGEMENTS

This work was partially supported by ANR JCJC project milliPICS, the Région Midi-Pyrénées under contract MESR 13053031, BLAPHENE project under IDEX program Emer-

gence

Methods

GaAs nanomembranes used in that study are grown with a DCA solid source Molecular Beam Epitaxy (MBE) system. Substrates are PECVD deposited SiO_2 masked (111)B GaAs. The oxide thickness is 30 nm. The growth mask is patterned with a combination of e-beam lithography and fluorine based dry etching as reported earlier.[43] The growth temperature is 635 °C, the growth rate is 1 Å/s and the V/III ratio is 10 for the GaAs core. The length of nanomembranes and the distance between them are defined by patterning the SiO_2 mask. We focused our characterization on structures having structures with 100 nm width, 500 nm pitch and 10μm length are studied. In the case of capped GaAs nanomembranes, the structures are capped with a shell of $Al_xGa_{1-x}As$. ($x = 0.15, 0.3$ and 0.5) The substrate temperature is reduced to 460 °C and As flux is increased to 1×10^{-5} torr for shell growth. Nominal thickness of AlGaAs shell is always 50 nm and it is protected with 10 nm of GaAs against oxidization. Aluminum ratios and nominal AlGaAs layer thicknesses are deduced from RHEED calibrations performed on (100) GaAs substrates.

For the measurements the samples were placed in a helium flow cryostat with optical access. The cryostat was mounted on the motorized $x-y$ translation stages, which allows high resolution spatial mapping. A microscope objective 50× with a numerical aperture NA = 0.55 was used to focus the excitation beam and collect the PL from the nano membranes. The laser spot could be focussed down to a diameter of $\simeq 0.5\mu$m (diffraction limit), which enabled us to optically address single (or a maximum of two in a worst case scenario). To investigate many membranes the laser spot was defocussed. The steady-state μPL signal was excited with a 532 nm laser and the spectra were recorded using a spectrometer equipped with a liquid nitrogen cooled CCD camera. All the measurements presented here have been performed at $T = 4.2$ K.

References

(1) Hu, J.; Odom, T. W.; Lieber, C. M. *Accounts of Chemical Research* **1999**, *32*, 435–445.

(2) Cui, Y.; Lieber, C. M. *Science* **2001**, *291*, 851.

(3) Thelander, C. *Mater. Today* **2006**, *9*, 28.

(4) Lieber, C. M.; Wang, Z. L. *MRS Bulletin* **2007**, *32*, 99–108.

(5) Lu, W.; Lieber, C. M. *Nature Mater.* **2007**, *6*, 841.

(6) Hua, B.; Motohisa, J.; Kobayashi, Y.; Hara, S.; Fukui, T. *Nano Letters* **2009**, *9*, 112–116, PMID: 19072060.

(7) Saxena, D.; Mokkapati, S.; Parkinson, P.; Jiang, N.; Gao, Q.; Tan, H. H.; Jagadish, C. *Nature Photonics* **2013**, *7*, 963–968.

(8) Atwater, H. A.; Polman, A. *Nature Materials* **2010**, *9*, 205–213.

(9) Wallentin, J.; Anttu, N.; Asoli, D.; Huffman, M.; Åberg, I.; Magnusson, M. H.; Siefer, G.; Fuss-Kailuweit, P.; Dimroth, F.; Witzigmann, B.; Xu, H. Q.; Samuelson, L.; Deppert, K.; Borgström, M. T. *Science* **2013**, *339*, 1057–1060.

(10) Krogstrup, P.; Jørgensen, H. I.; Heiss, M.; Demichel, O.; Holm, J. V.; Aagesen, M.; Nygard, J.; i Morral, A. F. *Nature Photonics* **2013**, *7*, 306–310.

(11) Mann, S. A.; Oener, S. Z.; Cavalli, A.; Haverkort, J. E. M.; Bakkers, E. P. A. M.; Garnett, E. C. *Nat Nano* **2016**, *advance online publication*.

(12) Tian, B.; Liu, J.; Dvir, T.; Jin, L.; Tsui, J. H.; Qing, Q.; Suo, Z.; Langer, R.; Kohane, D. S.; Lieber, C. M. *Nat Mater* **2012**, *11*, 986–994.

(13) Takei, K.; Takahashi, T.; Ho, J. C.; Ko, H.; Gillies, A. G.; Leu, P. W.; Fearing, R. S.; Javey, A. *Nat Mater* **2010**, *9*, 821–826.

(14) Nelson, R. J.; Sobers, R. G. *Applied Physics Letters* **1978**, *32*, 761–763.

(15) Schricker, A. D.; III, F. M. D.; Wiacek, R. J.; Korgel, B. A. *Nanotechnology* **2006**, *17*, 2681.

(16) Parkinson, P.; Lloyd-Hughes, J.; Gao, Q.; Tan, H. H.; Jagadish, C.; Johnston, M. B.; Herz, L. M. *Nano Letters* **2007**, *7*, 2162–2165.

(17) Demichel, O.; Heiss, M.; Bleuse, J.; Mariette, H.; Fontcuberta i Morral, A. *Applied Physics Letters* **2010**, *97*.

(18) Katzenmeyer, A. M.; Lonard, F.; Talin, A. A.; Wong, P. S.; Huffaker, D. L. *Nano Letters* **2010**, *10*, 4935–4938, PMID: 21053980.

(19) Calarco, R.; Marso, M.; Richter, T.; Aykanat, A. I.; Meijers, R.; v.d. Hart, A.; Stoica, T.; Lth, H. *Nano Lett.* **2005**, *5*, 981–984.

(20) Noborisaka, J.; Motohisa, J.; Hara, S.; Fukui, T. *Applied Physics Letters* **2005**, *87*.

(21) Chang, C. C.; Chi, C.-Y.; Yao, M.; Huang, N.; Chen, C. C.; Theiss, J.; Bushmaker, A. W.; LaLumondiere, S.; Yeh, T. W.; Povinelli, M. L.; Zhou, C.; Dapkus, P. D.; Cronin, S. B. *Nano Letters* **2012**, *12*, 4484–4489, PMID: 22889241.

(22) Mallorquí, A. D.; Alarcón-Lladó, E.; Mundet, I. C.; Kiani, A.; Demaurex, B.; De Wolf, S.; Menzel, A.; Zacharias, M.; Fontcuberta i Morral, A. *Nano Research* **2015**, *8*, 673–681.

(23) Yuan, Y. R.; Pudensi, M. A. A.; Vawter, G. A.; Merz, J. L. *Journal of Applied Physics* **1985**, *58*, 397–403.

(24) Dhaka, V.; Oksanen, J.; Jiang, H.; Haggren, T.; Nykänen, A.; Sanatinia, R.; Kakko, J.-P.; Huhtio, T.; Mattila, M.; Ruokolainen, J.; Anand, S.; Kauppinen, E.; Lipsanen, H. *Nano Letters* **2013**, *13*, 3581–3588.

(25) Smith, L. M.; Jackson, H. E.; Yarrison-Rice, J. M.; Jagadish, C. *Semiconductor Science and Technology* **2010**, *25*, 024010.

(26) Songmuang, R.; Giang, L. T. T.; Bleuse, J.; Hertog, M. D.; Niquet, Y. M.; Dang, L. S.; Mariette, H. *Nano Letters* **0**, *0*, null, PMID: 27081785.

(27) Hocevar, M.; Thanh Giang, L. T.; Songmuang, R.; den Hertog, M.; Besombes, L.; Bleuse, J.; Niquet, Y.-M.; Pelekanos, N. T. *Applied Physics Letters* **2013**, *102*, –.

(28) Heiss, M. et al. *Nature Materials* **2013**, *12*, 439.

(29) Mancini, L.; Fontana, Y.; Conesa-Boj, S.; Blum, I.; Vurpillot, F.; Francaviglia, L.; Russo-Averchi, E.; Heiss, M.; Arbiol, J.; Morral, A. F. i.; Rigutti, L. *Applied Physics Letters* **2014**, *105*.

(30) Heiss, M.; Conesa-Boj, S.; Ren, J.; Tseng, H.-H.; Gali, A.; Rudolph, A.; Uccelli, E.; Peiró, F.; Morante, J. R.; Schuh, D.; Reiger, E.; Kaxiras, E.; Arbiol, J.; Fontcuberta i Morral, A. *Phys. Rev. B* **2011**, *83*, 045303.

(31) Plissard, S.; Dick, K. A.; Larrieu, G.; Godey, S.; Addad, A.; Wallart, X.; Caroff, P. *Nanotechnology* **2010**, *21*, 385602.

(32) Thelander, C.; Caroff, P.; Plissard, S.; Dey, A. W.; Dick, K. A. *Nano Lett.* **2011**, *11*, 2424–2429.

(33) de la Mata, M.; Magen, C.; Gazquez, J.; Utama, M. I. B.; Heiss, M.; Lopatin, S.; Furtmayr, F.; Fernndez-Rojas, C. J.; Peng, B.; Morante, J. R.; Rurali, R.; Eickhoff, M.; i Morral, A. F.; Xiong, Q.; Arbiol, J. *Nano Letters* **2012**, *12*, 2579–2586, PMID: 22493937.

(34) Arbiol, J.; Estrad, S.; Prades, J. D.; Cirera, A.; Furtmayr, F.; Stark, C.; Laufer, A.; Stutzmann, M.; Eickhoff, M.; Gass, M. H.; Bleloch, A. L.; Peir, F.; Morante, J. R. *Nanotechnology* **2009**, *20*, 145704.

(35) Shtrikman, H.; Popovitz-Biro, R.; Kretinin, A.; Houben, L.; Heiblum, M.; Bukala, M.; Galicka, M.; Buczko, R.; Kacman, P. *Nano Letters* **2009**, *9*, 1506–1510, PMID: 19253998.

(36) Shtrikman, H.; Popovitz-Biro, R.; Kretinin, A.; Heiblum, M. *Nano Letters* **2009**, *9*, 215–219.

(37) Plochocka, P.; Mitioglu, A. A.; Maude, D. K.; Rikken, G. L. J. A.; Granados del Aguila, A.; Christianen, P. C. M.; Kacman, P.; Shtrikman, H. *Nano Letters* **2013**, *13*, 2442–2447.

(38) Yuan, X.; Caroff, P.; Wong-Leung, J.; Fu, L.; Tan, H. H.; Jagadish, C. *Advanced Materials* **2015**, *27*, 6096–6103.

(39) Chi, C.-Y.; Chang, C.-C.; Hu, S.; Yeh, T.-W.; Cronin, S. B.; Dapkus, P. D. *Nano Letters* **2013**, *13*, 2506–2515, PMID: 23634790.

(40) Arab, S.; Chi, C.-Y.; Shi, T.; Wang, Y.; Dapkus, D. P.; Jackson, H. E.; Smith, L. M.; Cronin, S. B. *ACS Nano* **2015**, *9*, 1336–1340, PMID: 25565000.

(41) Chang, C. C.; Chi, C. Y.; Chen, C. C.; Huang, N.; Arab, S.; Qiu, J.; Povinelli, M. L.; Dapkus, P. D.; Cronin, S. B. *Nano Research* **2014**, *7*, 163–170.

(42) de la Mata, M.; Leturcq, R.; Plissard, S. R.; Rolland, C.; Magn, C.; Arbiol, J.; Caroff, P. *Nano Letters* **2016**, *16*, 825–833, PMID: 26733426.

(43) Tutuncuoglu, G.; de la Mata, M.; Deiana, D.; Potts, H.; Matteini, F.; Arbiol, J.; Fontcuberta i Morral, A. *Nanoscale* **2015**, *7*, 19453–19460.

(44) Hei, M.; Riedlberger, E.; Spirkoska, D.; Bichler, M.; Abstreiter, G.; i Morral, A. F. *Journal of Crystal Growth* **2008**, *310*, 1049 – 1056.

(45) Woolf, D. A.; Sobiesierski, Z.; Westwood, D. I.; Williams, R. H. *Journal of Applied Physics* **1992**, *71*, 4908–4915.

(46) Heim, U.; Hiesinger, P. *physica status solidi (b)* **1974**, *66*, 461–470.

(47) Kunzel, H.; Ploog, K. *Applied Physics Letters* **1980**, *37*, 416–418.

(48) Zhang, G.; Tateno, K.; Sanada, H.; Tawara, T.; Gotoh, H.; Nakano, H. *Applied Physics Letters* **2009**, *95*.

(49) Ploog, K.; Dhler, G. H. *Advances in Physics* **1983**, *32*, 285–359.

(50) van Weert, M. H. M.; Wunnicke, O.; Roest, A. L.; Eijkemans, T. J.; Yu Silov, A.; Haverkort, J. E. M.; t Hooft, G. W.; Bakkers, E. P. A. M. *Applied Physics Letters* **2006**, *88*.

(51) Signorello, G.; Karg, S.; Bjrk, M. T.; Gotsmann, B.; Riel, H. *Nano Letters* **2013**, *13*, 917–924, PMID: 23237482.

(52) Oskooi, A. F.; Roundy, D.; Ibanescu, M.; Bermel, P.; Joannopoulos, J. D.; Johnson, S. G. *Computer Physics Communications* **2010**, *181*, 687–702.

(53) Adachi, S. *Journal of Applied Physics* **1985**, *58*, R1–R29.